(10) do not have a sound mathematical justification, the results are surprisingly accurate, not only for the fundamental frequency, but also for the overtone frequencies for a range of Timoshenko beams.

References

[1]Abramovich, H., and Elishakoff, I., "Influence of Shear Deformation and Rotary Inertia on Vibration Frequencies via Love's Equation," *Journal of Sound and Vibration*, Vol. 137, No. 3, 1990, pp. 516–522.

[2]Chandrasekhara, K., Krishna Murthy, K., and Roy, S., "The Vibration of Composite Beams Including Rotary Inertia and Shear Deformation," *Composite Structures*, Vol. 14, No. 4, 1990, pp. 269–279.

[3]Peters, D. A., "An Approximate Solution for the Free Vibration of Rotating Uniform Cantilever Beams," NASA TMX-62299, Sept. 1973.

[4]Stafford, R. D., and Giurgiutiu, V., "Semi-Analytic Methods for Rotating Timoshenko Beams," *International Journal of Mechanical Sciences*, Vol. 17, Nos. 11–12, 1975, pp. 719–727.

[5]Cowper, G. R., "The Shear Coefficient in Timoshenko's Beam Theory," *Journal of Applied Mechanics*, Vol. 33, June 1966, pp. 335–340.

Pitch Rate Effects on Delta Wing Vortex Breakdown

Lars E. Ericsson*
Mountain View, California 94040

Introduction

THE increasing performance demands on advanced aircraft, including maneuvers at high angles of attack, has led to a need for the prediction of vehicle aerodynamics that are dominated by unsteady separated flow effects. For aircraft with highly swept wing leading edges the challenge is to fully understand the unsteady flow physics behind the observed dramatic effects of vortex breakdown. In this Note, an attempt is made to pinpoint the fluid–mechanical processes that are causing the unpredicted large dynamic effects of high-rate/large-amplitude pitch oscillations on delta wing vortex breakdown.

Discussion

The pitching[1] and rolling[2] motions of delta wing aircraft have been found to have a large impact on the vortex breakdown characteristics. The fluid mechanics behind the surprisingly large pitch-rate-induced effects will be examined in what follows. The case of roll oscillations was analyzed in Refs. 3 and 4 for a 65-deg delta wing.

The vortex breakdown on a pitching 52-deg delta wing has been investigated by Atta and Rockwell[5] (Figs. 1 and 2). To quote the authors:

> There are several striking features of the vortex development and breakdown. First, the maximum extent of the laminar vortex core occurs near the maximum angle of attack (see photo C), rather than near the minimum angle of attack, which is in direct contradiction to what one would expect on the basis of quasisteady behavior.

Presented as Paper 95-0367 at the AIAA 33rd Aerospace Sciences Meeting and Exhibit, Reno, NV, Jan. 9–12, 1995; received Feb. 15, 1995; revision received Jan. 5, 1996; accepted for publication Jan. 10, 1996.

*Engineering Consultant. Fellow AIAA.

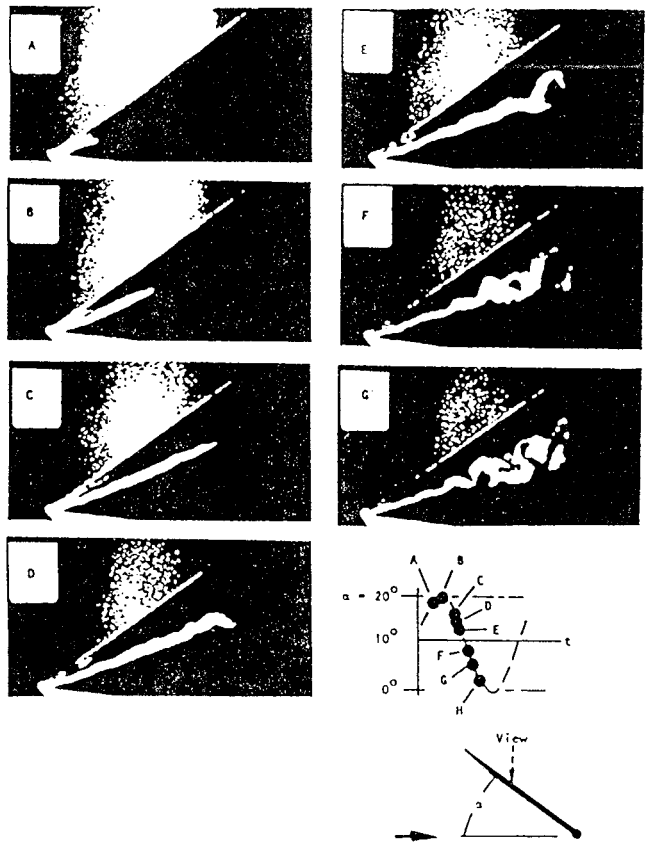

Fig. 1 Visualization of vortex breakdown on an oscillating 52-deg swept wing, $\alpha_0 = 10$ deg, $\Delta\alpha = 10$ deg, and $\bar{\omega} = 1.52$ (Ref. 5).

It is true that the local, instantaneous flow conditions, as defined in the classic quasisteady approach, cannot explain this dynamic deviation from the static vortex characteristics. However, it will be shown that when the definition of time-lagged, quasisteady characteristics used in Ref. 6 is extended to include the effects of rate-induced camber, the large dynamic effects in Figs. 1 and 2 can be explained. These dynamically equivalent steady (DES) characteristics, a nomenclature suggested by Beyers[7] to distinguish them from the classic quasisteady characteristics, will be described in what follows.

The classic, quasisteady (instantaneous) angle of attack is

$$\alpha = \alpha(t) - \dot{\alpha}(t)(x_{TE} - x)/U_\infty \tag{1a}$$

$$\alpha(t) = \alpha_0 + \Delta\alpha \sin \omega t \tag{1b}$$

$$\dot{\alpha}(t) = \Delta\alpha\omega \cos \omega t \tag{1c}$$

At the apex $x = x_A = 0$, and with $x_{TE} = c$, Eq. (1) gives

$$\alpha_A(t) = \alpha_0 + \Delta\alpha \sin \omega t - \Delta\alpha\bar{\omega} \cos \omega t \tag{2}$$

where, in the present case, $\alpha_0 = \Delta\alpha = 10$ deg and $\bar{\omega} = \omega c/U_\infty = 1.52$.

The development of a leading-edge vortex on the top side starts when the angle of attack at the apex exceeds $\alpha_A(t) = 0$. During the upstroke, $\dot{\alpha} > 0$, Eqs. (1) and (2) show that this value is reached when $\omega t = 23.2$ deg, where according to Eq. (1), $\alpha(t) = 13.9$ deg. The corresponding experimental value for $\xi = x/c = 0$ in Fig. 2 is $\alpha(t) = 17$ deg. According to Ref. 8, the difference between prediction and experiment could in part have been caused by the blunted 10-deg wedge shape of the leading edge. Another contributing cause is the following: Eq. (2) shows that $\alpha_A(t)$ starts at zero for $\omega t = -90$ deg, and reaches a peak negative value of -8.2 deg at $\omega t = -33.6$ deg and -5.2 deg at $\omega t = 0$, before finally reaching $\alpha_A(t) = 0$ at $\omega t = 23.2$ deg (Fig. 3). Thus, when $\alpha_A(t) > 0$ and leading-edge

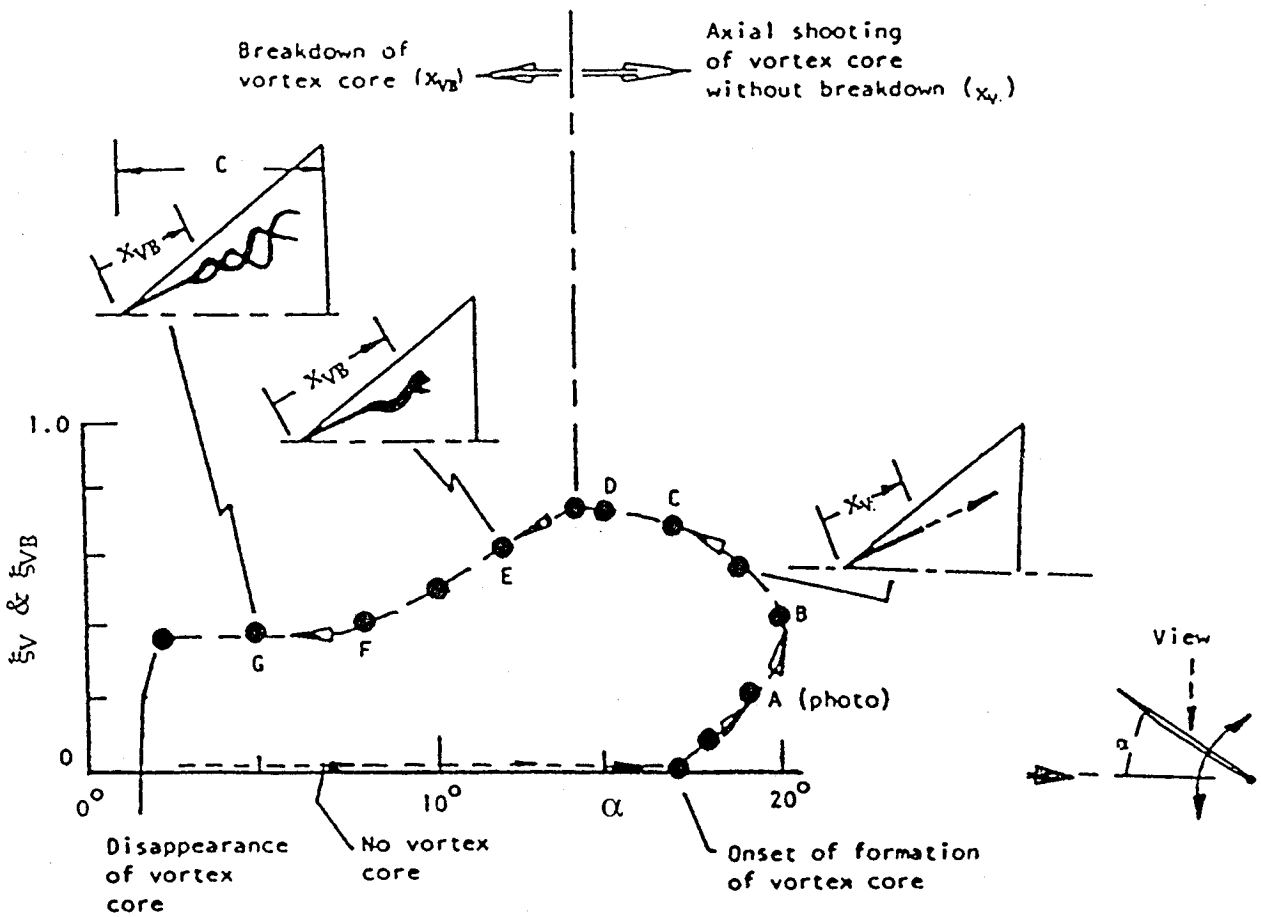

Fig. 2 Vortex development on an oscillating 52-deg delta wing, $\alpha_0 = 10$ deg, $\Delta\alpha = 10$ deg, and $\bar{\omega} = 1.52$ (Ref. 5).

vortices can start developing on the top side, leading-edge vortices of the opposite sign exist on the bottom side. This probably also accounts for some of the differences between the predicted and experimental α values in Fig. 3 for starting development of the leading-edge vortex on the top side.

For $\xi = x/c > 0$, the effect of time lag on the vortex development has to be included in Eq. (1).

$$\alpha(t - \Delta t) = \alpha_0 + \Delta\alpha \sin(\omega t - \omega\Delta t) \tag{3a}$$

$$\Delta t = c\xi/\bar{U} \tag{3b}$$

For a 70-deg delta wing, experimental results[9] gave $\bar{U}/U_\infty \approx 4/3$. In this case the difference between x_V and x was negligible (see insert in Fig. 2). In the present case of the 52-deg delta wing, this is not true. According to measurements[10] the spanwise location η_V of the vortex can be defined as follows[11] ($\theta_{LE} = \pi/2 - \Lambda$):

$$\eta_V = 0.56 + 0.36/(1.75 + \alpha/\theta_{LE}) \tag{4}$$

Equation (4) shows that $\eta_V \approx 0.75$ is a representative value for the 52-deg delta wing, giving $\theta_V = 30.3$ deg and $x_V/x = \sec 30.3$ deg $= 1.17$. Thus, the velocity $\bar{U} = 1.33U_\infty$ along the x_V axis corresponds to $\bar{U} = 1.14U_\infty$ along the x axis. The corresponding prediction of $\alpha(t - \Delta t)$ as a function of ξ is shown by the dash–dot curve in Fig. 3. Note that according to the analysis in Ref. 6, the DES concept is valid as long as the axial vehicle extent is less than the quarter wavelength of the oscillation, i.e., $\bar{\omega} < \pi/2$. In the present test[5] (Figs. 1–3), $\bar{\omega} = 1.52 < \pi/2$.

The pitch-rate-induced camber (Fig. 4) can be expected to have a dramatic effect on vortex breakdown judging by the experimental results[12] in Fig. 5. The static camber in Fig. 5 is

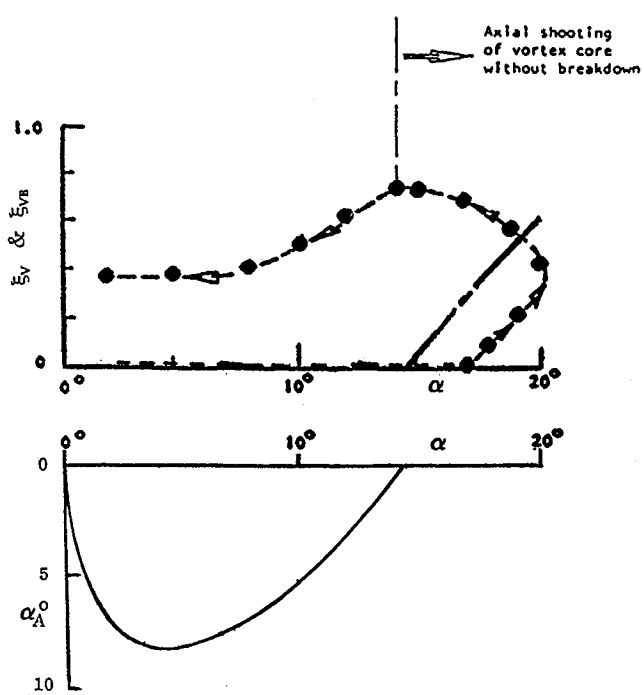

Fig. 3 Initial vortex development.

$\Delta\alpha_c/\alpha_{max} = \pm 1$, where $|\Delta\alpha_c| = \alpha_{max} = 5$ deg. For the pitching delta wing in Fig. 2, the pitch-rate-induced equivalent steady camber is $\Delta\alpha_c = \Delta\alpha\bar{\omega}\cos\omega t$. That is, $\Delta\alpha_c/\alpha_{max} = [\Delta\alpha\bar{\omega}/(\alpha_0 + \Delta\alpha)]\cos\omega t = 0.756\cos\omega t$. Thus, the magnitude of the pitch-rate-induced camber in Fig. 2 is almost as large as that of the static camber in Fig. 5.

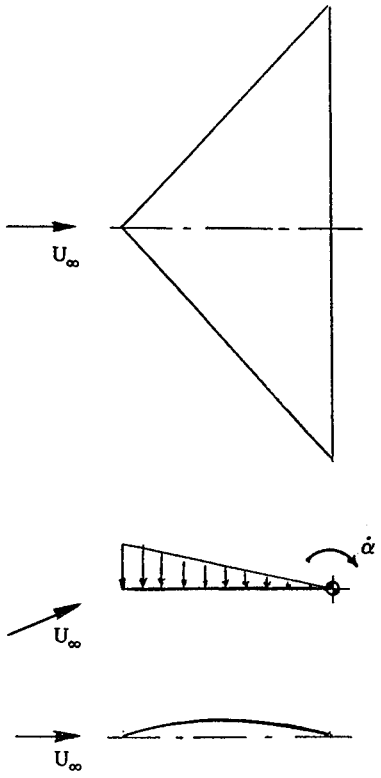

Fig. 4 Pitch-rate-induced camber.

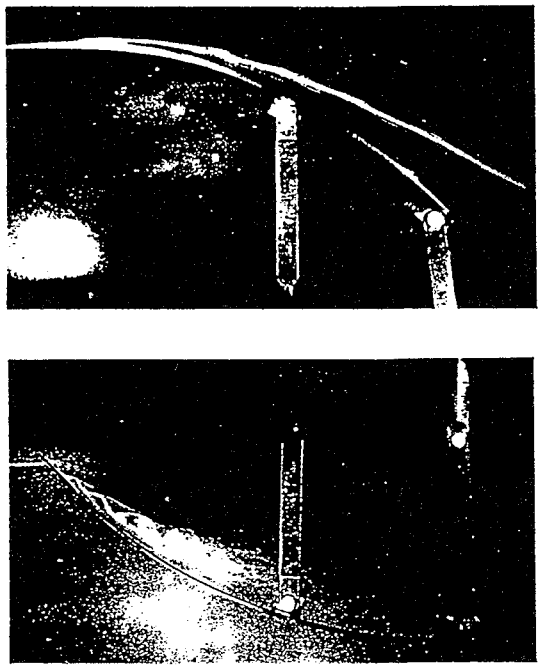

Fig. 5 Leading-edge vortex characteristics on an 80-deg delta wing.[12] Local incidence a) increasing and b) decreasing with x.

The maximum camber $\Delta\alpha_c$ = 15.2 deg, generated on the upstroke at $\alpha = \alpha_0$ = 10 deg (Fig. 6), is realized at a time increment $\Delta t = c\xi/\bar{U}$ later, when the phase angle is $\omega\Delta t = \bar{\omega}\xi/1.17$. At ξ = 0.7 the phase angle is ωt = 52 deg and α is 17.85 deg according to Eq. (1b). That is consistent with the observed absence of vortex breakdown during the upstroke[5] (α < 10 deg in Fig. 3). At α = 20 deg, the pitch-rate-induced camber effect changes from the positive, breakdown-delaying kind during the upstroke to the negative, breakdown-promoting kind for the downstroke. In the test[5] this change was felt by the vortex at $\xi \approx 0.7$ when $\alpha \approx$ 14 deg (Fig. 3). At these

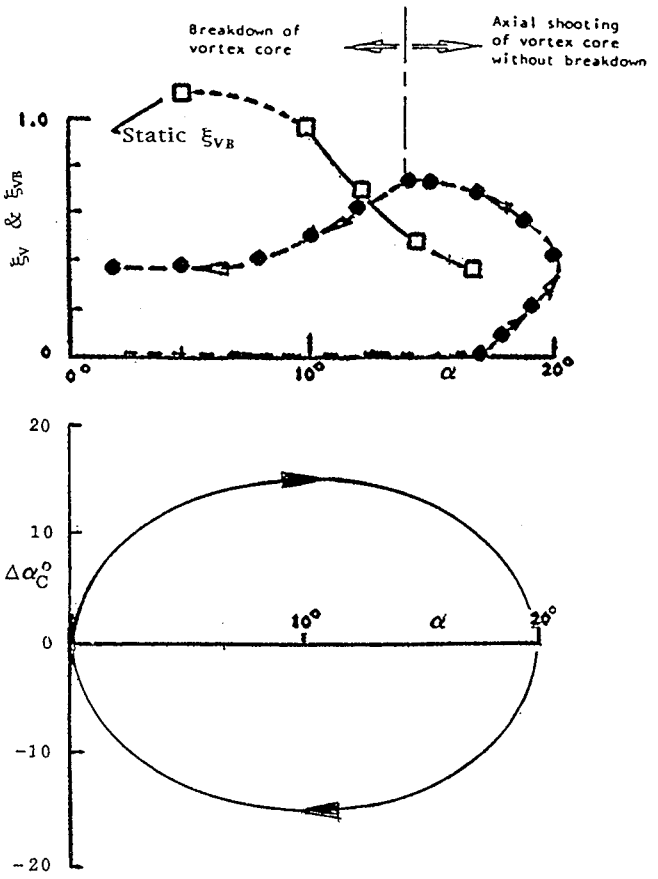

Fig. 6 Pitch-rate-induced camber effect on an oscillating 52-deg delta wing.

conditions the following relationship is obtained for the determination of the time lag Δt_{VB} associated with the effect of the rate-induced camber on the vortex breakdown

$$\alpha(t) = \alpha_0 + \Delta\alpha \sin(\pi/2 - \omega\Delta t_{VB}) \tag{5}$$

With $\alpha(t)$ = 14 deg and $\alpha_0 = \Delta\alpha$ = 10 deg, Eq. (5) gives $\omega\Delta t_{VB}$ = 76 deg. Comparing it with the time-lag effect on the vortex formation, $\omega\Delta t_V = \omega\xi = \bar{\omega}\xi/1.17 = 1.52 \times 0.7 = 52$ deg, gives the ratio $\omega\Delta t_V/\omega\Delta t_{VB} = 0.685$. The maximum breakdown-promoting camber effect during the downstroke, generated at α = 10 deg, when $\omega t = \pi$, is felt a time increment Δt_{VB} later, when α = 10 deg (1 − sin 76 deg) = 0.3 deg. This agrees well with the experimental result in Fig. 3, showing the vortex breakdown progressing to its most forward position when the angle of attack approaches zero during the downstroke. Thus, the effect of the pitch-rate-induced camber on vortex breakdown is associated with a significantly larger time lag than $\Delta t = \xi c/\bar{U}$. This is fully in agreement with existing experimental results. [The extremely large time lags and associated very low convection velocities reported by some investigators is the likely result of representing the rate-induced camber effect by an additional time lag for $\alpha(t)$.]

References

[1]LeMay, S. P., Batill, S. M., and Nelson, R. C., "Leading Edge Vortex Dynamics on a Pitching Delta Wing," AIAA Paper 88-2559, June 1988.

[2]Hanff, E. S., and Jenkins, S. B., "Large-Amplitude High-Rate Roll Experiments on a Delta and Double Delta Wing," AIAA Paper 90-0224, Jan. 1990.

[3]Ericsson, L. E., "Flow Physics of Critical States for Rolling Delta Wings," *Journal of Aircraft*, Vol. 32, No. 3, 1995, pp. 603–610.

[4]Ericsson, L. E., "Difficulties in Predicting Vortex Breakdown Effects on a Rolling Delta Wing," *Journal of Aircraft*, Vol. 33, No. 3, 1996, pp. 477–484.
[5]Atta, R., and Rockwell, D., "Hysteresis of Vortex Development and Breakdown on an Oscillating Delta Wing," *AIAA Journal*, Vol. 25, No. 11, 1987, pp. 1512, 1513.
[6]Ericsson, L. E., and Reding, J. P., "Fluid Dynamics of Unsteady Separated Flow, Part II, Lifting Surfaces," *Progress in Aerospace Sciences*, Vol. 24, 1987, pp. 249–356.
[7]Beyers, M. E., private communication, July 1994.
[8]Ericsson, L. E., and King, H. H. C., "Effect of Cross-Sectional Geometry on Slender Wing Unsteady Aerodynamics," *Journal of Aircraft*, Vol. 30, No. 5, 1993, pp. 793–795.
[9]Lambourne, N. C., Bryer, D. W., and Maybrey, J. F. M., "The Behavior of the Leading Edge Vortices over a Delta Wing Following a Sudden Change of Incidence," Aeronautical Research Council, R&M 3645, England, UK, March 1969.
[10]Elle, B. J., "An Investigation at Low Speed of the Flow near the Apex of Thin Delta Wings with Sharp Leading Edges," Aeronautical Research Council, R&M 3176, England, UK, Jan. 1958.
[11]Ericsson, L. E., and Reding, J. P., "Approximate Nonlinear Slender Wing Aerodynamics," *Journal of Aircraft*, Vol. 14, No. 12, 1977, pp. 1197–1204.
[12]Lambourne, N. C., and Bryer, D. W., "The Bursting of Leading-Edge Vortices—Some Observations and Discussion of the Phenomenon," Aeronautical Research Council, R&M 3282, England, UK, April 1961.

Numerical Approach to Blade–Vortex Interaction in Two-Dimensional Viscous Flow

Bonian Dong*
Singapore Technologies Aerospace, 539938 Singapore
and
Y. T. Chew† and B. C. Khoo‡
National University of Singapore, 119260 Singapore

Introduction

In the previous two-dimensional viscous study on the blade–vortex interaction, the total flowfield is obtained through the interaction between the vortex-induced flow and the viscous flow around the stationary airfoil.[1,2] The shortcoming of such an interaction scheme is that the viscous effect of the passing vortex is not taken into consideration in the viscous solution. The purpose of this work is to introduce a numerical approach that includes the passing vortex in the viscous solution. The calculation is started in a manner similar to the one used by Wu et al.[1] and Hsu and Wu,[2] except that, in this work, the passing vortex is modeled as a cluster of point vortices. Based on the concept of the vortex-in-cell (VIC) method for inviscid flows,[3] a specially devised vorticity distribution scheme is used when the passing vortex is close to the stationary airfoil. In this scheme, the cluster of point vortices becomes a continuous vortical patch after being linearly distributed in a weighted manner. Then the total flow is solved by the Navier–Stokes equations, and the viscous effect of the passing vortex on the blade–vortex interaction can be investigated.

Received June 26, 1994; revision received Nov. 1, 1995; accepted for publication Dec. 10, 1995.

*Research Engineer, Engineering Development Center.
†Associate Professor, Department of Mechanical and Production Engineering.
‡Senior Lecturer, Department of Mechanical and Production Engineering.

Equations and Numerical Schemes

The problem is stated as follows: the steady flowfield around a stationary airfoil is disturbed by a passing vortex released from upstream, and then the resulting unsteady flowfield is studied.[2]

The unsteady incompressible Navier–Stokes equations in the form of a vorticity-stream function for two-dimensional flows are

$$\frac{\partial^2\psi}{\partial x^2}+\frac{\partial^2\psi}{\partial y^2}=-\omega$$
$$\frac{\partial\omega}{\partial t}+\frac{\partial\psi}{\partial y}\frac{\partial\omega}{\partial x}-\frac{\partial\psi}{\partial x}\frac{\partial\omega}{\partial y}=\frac{1}{Re}\left(\frac{\partial^2\omega}{\partial x^2}+\frac{\partial^2\omega}{\partial y^2}\right) \tag{1}$$

where ψ is the stream function, ω is the vorticity, and Re is the Reynolds number based on the airfoil chord length and freestream velocity. On the solid wall, the boundary conditions are

$$\psi_w=0$$
$$\omega_w=-\left.\frac{\partial^2\psi}{\partial n^2}\right|_w\approx-\frac{2(\psi_1-\psi_w)}{h^2} \tag{2}$$

where n is the local normal coordinate, and the subscripts w and 1 indicate the wall and the first point at the distance of h from the wall, respectively. The first-order discretization for ω in Eq. (2) is used in the numerical solution to keep the total vorticity of the flow conserved as discussed by Wu.[4] On the far-field boundary, ω and ψ take the values of the freestream. The linear triangular finite element method[5] on a C-grid is used to calculate the viscous flow surrounding the stationary airfoil, and no artificial viscosity is applied.

Interaction Scheme

This scheme is similar to the one used by Wu et al.[1] and Hsu and Wu,[2] who used only one point vortex to represent the passing vortex, but in this work, a cluster of point vortices is used.[6] The stream function of total flow can be decomposed as two parts: 1) the vortex-induced flow ψ_Γ and 2) the disturbed viscous flow ψ_V. Here, ψ_Γ is evaluated by the Biot–Savart law[1] and ψ_V is solved by substituting $\psi=\psi_V+\psi_\Gamma$ into Eq. (1) and utilizing the boundary conditions. The passing vortex is made to convect at the local fluid speed. In this scheme, the passing vortex is not included in the viscous solution.

Distribution Scheme

In the linear triangular finite element calculation, ω_0 at a node represents a linear vorticity distribution on the six elements that share the same node as shown in Fig. 1a, and the circulation (positive clockwise) around these six elements is

$$\Gamma_0(\omega_0)=-\frac{\omega_0}{3}\sum_{k=1}^{6}A_k \tag{3}$$

where A_k is the area pertaining to element k as shown in Fig. 1a. For a point vortex located in an element, its vorticity strength is approximated by ω_1, ω_2, and ω_3 at the three nodes of the element. In this way, the point vortex becomes a vortical patch occupying the element where it is located and also the 12 adjacent elements as shown in Fig. 1b. The values of ω_1, ω_2, and ω_3 are weighted as follows:

$$\omega_1/a_1=\omega_2/a_2=\omega_3/a_3 \tag{4}$$

where a_1, a_2, and a_3 are subareas of the element as shown in